J. Appl. Comput. Mech., 7(1) (2021) 355-371
DOI: 10.22055/JACM.2020.35156.2580

ISSN: 2383-4536
jacm.scu.ac.ir

Shahid Chamran University of Ahvaz

Journal of Applied and Computational Mechanics

Research Paper

Measuring Crack-type Damage Features in Thin-walled Composite Beams using De-noising and a 2D Continuous Wavelet Transform of Mode Shapes

Josué Pacheco-Chérrez[1], Diego Cárdenas[2], Oliver Probst[3]

[1] Tecnologico de Monterrey, School of Engineering and Sciences, Av. Eugenio Garza Sada 2051 Sur, Monterrey , CP64849, Mexico, Email: a00824133@itesm.mx

[2] Tecnologico de Monterrey, School of Engineering and Sciences, General Ramón Corona 2514, CP 45138, Zapopan, Mexico, Email: diego.cardenas@tec.mx

[3] Tecnologico de Monterrey, School of Engineering and Sciences, Av. Eugenio Garza Sada 2051 Sur, Monterrey , CP64849, Mexico, Email: oprobst@tec.mx

Received September 24 2020; Revised November 06 2020; Accepted for publication November 06 2020.
Corresponding author: Oliver Probst (oprobst@tec.mx)

Abstract. A new method is described, allowing to locate and also measure the length and orientation of crack-type damage features in thin-walled composite beams (TWCB), a capability not previously reported. The method is based on a modal-analysis technique and is shown to work on a hollow composite beam, going beyond previous work limited to simple beams and plates. The method is shown to be capable to function down to signal-to-noise ratios (SNR) of about 15, corresponding to far noisier conditions than in most previous work. This capability is achieved by a combination of wavelet de-noising and the use of a 2D Continuous Wavelet Transform (CWT), applied to two modal analysis metrics, COMAC and Mode Shape Differences (MSD). The length and orientation of the crack can be determined accurately using a 2D curve fitting approach. Using either COMAC or MSD produces reliable results, but MSD is found to be somewhat more noise-tolerant. The new method is believed to be useful for the measurement of damage features in a variety of thin-walled composite beams such as aircraft wings and wind turbine blades, among others.

Keywords: Modal analysis; Damage detection; Damage assessment; 2D curve fitting.

1. Introduction

Composite laminates have been extensively applied in many engineering fields [1], due to their high specific stiffness and strength, low weight, corrosion resistance, and non-conductivity [2]. However, under various working conditions, or after long-term operation the structural integrity of composites structures could be affected. Therefore, structural health monitoring (SHM) techniques for damage detection and location are an important aspect of structural integrity assessment, e.g. for modern wind turbines [3]. In SHM, vibration-based damage detection has been one of the most widely applied non-destructive methods [4]. Vibration-based methods (VBM) are accurate, non-destructive, and inexpensive. If applied to SHM, VBM allow for the evaluation of the state of health of a structure by analyzing its dynamic response [5]. Structural damage can cause changes in structural stiffness, and further change the structural modal parameters [1]; [6]. A number of approaches have used Modal Assurance Criteria (MAC) and Coordinate Modal Assurance Criteria (COMAC) as convenient metrics for mode shape comparison, quantifying the degree of consistency between mode shapes [7]. Both metrics are therefore natural candidates for identifying damage in a mechanical structure by detecting deviations from an ideal mode shape. Methods based on the MAC metric have been reported to be able to detect the presence of damage, whereas COMAC has been shown to also locate damage features [8]. Altunışık et al. [9] calculated and measured natural frequencies and mode shapes for undamaged and damaged beams with a hollow circular cross-section. MAC and COMAC factors were obtained from the mode shapes and criteria for damaged location identification were established. However, damage features in mode shapes can easily be masked by noise, limiting the usefulness of the direct application of the MAC and COMAC methods to relatively large damage features [10]. For small damages, singularities in mode shapes arising from damage features can be detected and located more easily using some version of the wavelet transform, since small singularities in the mode shapes cause substantial variations in the wavelet coefficients [11]. A number of works have exploited this general idea, though so far mostly on one-dimensional test systems [12]; [13]; [14]; [15]. On the other hand, few works use the 2D wavelet transform. More recently, a few groups of authors have demonstrated the applicability of this approach to 2D samples. Abdulkareem et al. [4] used a 2D Continuous Wavelet Transform (CWT) to detect damage in steel plate structures. Wei Xu et al. [16] used the complex-wavelet 2D modal curvature (MC) method to eliminate noise and characterize non-uniform cracks under noisy conditions in plate-like structures. A limitation of the method was a rather high signal-to-noise (SNR) ratio of 65 dB required for damage detection. Makki et al. [17] were able to improve upon this SNR limit by using a somewhat different

Published online: November 10 2020

approach, based on a 2D Discrete Wavelet Transform (DWT) of the frequency response functions (FRF) of the damaged structure. The authors used the horizontal detail coefficients to localize damage up to noise levels of 5%, equivalent to a SNR of 26 dB. Yang and Oyadiji [18] combined Modal Frequency Surfaces (MFS) and 2D-CWT for damage detection in 2D composite laminate plates. The authors were able to demonstrate that delamination events could be detected with their method. A compilation of the recent work in the field has been shown in Table 1.

Even though damage detection methods based on the combination of modal analysis with wavelet transform techniques have attracted considerable attention in recent years, the field still seems to be rather incipient. Firstly, the majority of recent work still focuses on one-dimensional structures; see Table 2. Secondly, most of the published work on two-dimensional structures is limited to simple structures such as metal plates; the authors have only located one exception [18]. Thirdly, most published approaches are not very noise-tolerant, i.e. they require high signal-to-noise ratios to be successful. This is illustrated by the sixth column of Table 2, where only one exception [4] stands out in this respect. Finally, to the best knowledge of the authors no technique reported in literature seems to be able to yield information about geometric aspects, such as the length and orientation of a crack-type damage feature; see the fourth column of Table 2. The present work improves on all four of these shortcomings.

Regarding the test object, the present work uses a hollow (thin-walled) cylinder with an elliptical base area, made from fiber-reinforced polymer composite material. This test system can be viewed as a simplified version of a wind turbine blade or composite beam for structural applications, and therefore adds a realistic perspective to the study. As far as noise tolerance is concerned, it will be shown that the approach described in this work works down to SNR levels of 15 dB, which is comparable to the current state of the art [4]. And finally, a completely new capability is introduced, the one to measure the length and orientation of a crack-type damage feature.

The present work is organized as follows: Section 2 provides a brief overview of the methodology, followed by a in description of the setup of the FE-based computer experiments in section 3. Section 4 walks the reader through the different steps of the main steps used in this work to detect and locate damage. Section 5 introduces the surface fitting approach used to assess the length and orientation of crack-type faults and provides a comprehensive assessment. Section 6 provides some discussion of the results obtained. Section 7 summarizes the findings and points to some future work.

2. Methodology Overview

Fig. 1 presents a graphic summary of the methodology used in this work, which consists of six main stages. In the finite-element stage, the simulation of the geometry used in this work was carried out, the properties of the materials were loaded, and the modal information (mode shapes and frequencies) was extracted. The next stage is the detection of damage through COMAC and mode shape differences (MSD) for noise-free signals. Then the effect of noise was analyzed, for which noise of different SNR levels was added to the mode shapes. Subsequently, a noise elimination procedure using wavelets with three main stages was carried out: decomposition, threshold detail coefficients, and reconstruction. In the next stage, a wavelet transform in 2D was applied to the results of the wavelet de-noising. Different scale levels were analyzed, with the mother wavelet being the derivative of Gaussian in all cases. In the final step, an evaluation of the size and inclination of the fault is presented using the parameters resulting from the fitting of a bi-Gaussian surface.

Table 1. Overview of the recent literature.

Reference	Ref. #	Description
(He et al., 2017)	[1]	Nondestructive identification method for composite beams (Carbon fiber TR50).
(Zhu et al., 2019)	[15]	A damage index for the crack identification of FGM beams is introduced. The damage index was employed to identify the accurate position of the crack and reduce the edge effect.
(Manoach et al., 2017)	[5]	A Poincare map based damage index is presented for damage detection and location in composite beams.
(Zhang et al., 2020)	[8]	The COMAC and modal curvature indexes were applied to identify the damage of a ship under different conditions using numerical experiments.
(Altunışık et al., 2017)	[9]	Modal parameter identification and vibration-based damage detection of a cantilever beam with hollow circular section and multiple cracks.
(Shahsavari et al., 2017)	[11]	A principal component analysis was first performed to identify the most important patterns of variation in the wavelet coefficients and to minimize the effect of noise.
(Swamy et al., 2017)	[12]	Damage identification in beam structures based on continuous wavelet transform (CWT). The input to the CWT is the spatial signal of the displacement mode shapes.
(Serra and Lopez, 2017)	[14]	Mode shape de-noising by SWT, and the results are the input to a 1D-CWT. Wavelet transform coefficients serve as damage indices, which are standardized according to a statistical hypothesis approach.
(Janeliukstis et al., 2017)	[13]	Experimental validation of the applicability of a mode shape based spatial (CWT) technique and the MSCS method for detection and localization of damage in a beam structure.
(Skov et al., 2013)	[19]	Non-uniform crack identification in plate-like structures. A complex-wavelet 2D modal curvature approach was shown to be capable of simultaneously eliminating noise and characterizing cracks.
(Makki et al., 2015)	[17]	Damage detection and localization scheme using frequency response functions (FRFs) of the damaged structure. A 2-D discrete wavelet transform (DWT) working on measured FRFs of the damaged structure is used.
(Abdulkareem et al., 2019)	[3]	The mode shape difference of a square steel plate was subjected to WT decomposition. At high noise levels, the damage needs to be substantial to be detected; boundary conditions shown to be critical.
(Yang and Oyadiji, 2017)	[18]	A vibration-based damage detection method for composite laminate plates using 2D-WT is investigated through numerical examples with delaminations of various sizes and different thickness (depth) positions.

Table 2. Characteristics of recent work in the field. Abbreviations: LR Likelihood ratio; MSCS Mode shape curvature squares; SWT Stationary wavelet analysis; CW-MC Complex wavelet-modal curvature; AWGN Additive white Gaussian noise; CMD Curvature mode difference; FGM Functionally Graded Materials; CWT Continuous Wavelet Transform; WN White Noise; MC Modal Curvature; NN Neural Networks; PCA Principal Component Analysis; UDRN Uniformly Distributed Random Noise; MFS Modal Frequency Surface.

Ref.	Structure	Dim.	Size ass.	Noise Analysis	Minimum SNR [dB]	De-noising	Method
[1]	Composite cantilever beam	1D	No	No	-	No	CMD
[15]	Homogeneous cantilever beam	1D	No	WN	60, 46, 40	No	CWT
[5]	Composite beams	1D	No	No	-	No	Poincare map
[8]	Girder of a ship	1D	No	No	-	No	COMAC, MC, NN
[9]	Cantilever beam w/ hollow circ. cross-section	1D	No	No	-	No	MAC, COMAC
[11]	Steel beam	1D	No	No	-	PCA	CWT. LR
[12]	Free-free beam	1D	No	No	-	No	CWT
[14]	Cantilever steel beam	1D	No	WN	-	SWT	CWT, DWT
[13]	Aluminium & carbon/epoxy composite beams	2D	No	UDRN	28	No	CWT, MSCS
[19]	Aluminum plate	2D	No	Yes	65	No	CW-MC
[17]	Two-fixed-end steel beam	2D	No	AWGN	34, 26	DWT	DWT
[3]	Steel plate structures	2D	No	AWGN	34, 19, 18, 14	No	CWT
[18]	Composite laminate plates	2D	No	UDRN	-	No	MFS-CWT

3. Finite-element Modeling and Simulation Set-up

All results shown in this work were obtained with a set of computer experiments based on finite-element simulation. For damage detection, a hollow elliptical cylinder made from composite material, representing a typical thin-walled structure, was used; see Fig. 2. Modal analysis was used to extract the natural frequencies and mode shapes of the structure using the academic version of the commercial finite-element (FE) modeling software ANSYS 19. The elliptical cylinder shown in Fig. 2 has the following dimensions: a major axis of 100 mm, a minor axis of 60 mm, and a length of 585 mm. The walls of the cylinder have a layer structure of $[0/90]_{2s}$, with each layer having a thickness of 2 mm. The material properties employed in the FE analysis are given in Table 3. A simple meshing was carried out with the smooth transition option of ANSYS, and 6576 elements with 6541 nodes were obtained. For each node the 3 components of the displacement modes were calculated (x, y, z coordinates), from which their magnitude was obtained.

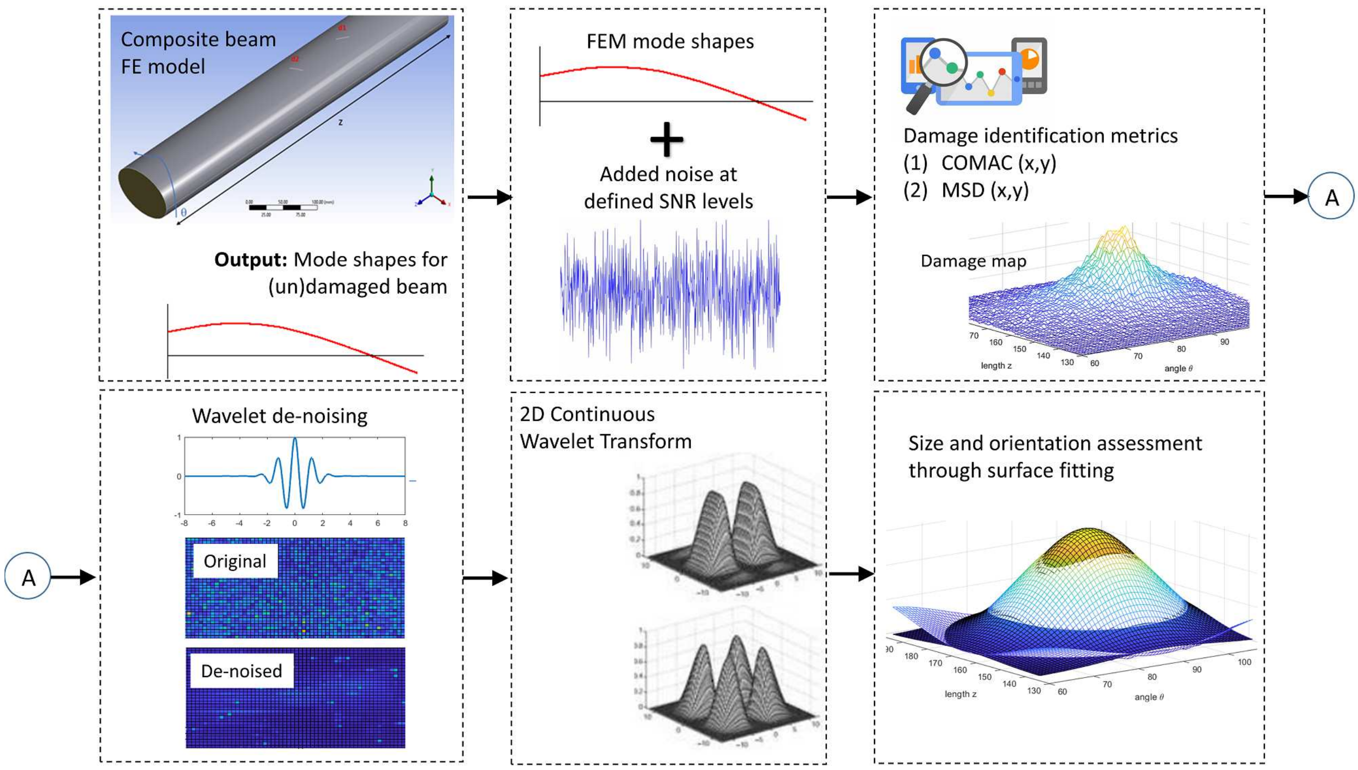

Fig. 1. Graphical overview of the methodology used in the present work.

Table 3. Materials properties used in this work.

Property	Parameters	Value	Unit
Elasticity modulus	E11	32.296	Gpa
	E22 = E33	13.971	GPa
Shear modulus	G12	6.987	GPa
	G13 = G23	5.756	GPa
Poisson's ratio	v12	0.262	-
	v13=v23	0.312	-

Table 4. Locations of the crack-type faults studied in this work.

Fault type	Shortcut	Location (θ) [°]	Location (z) [mm]
Transverse	t_1	71.21 - 108.78	180
Longitudinal	l_1	90	159 - 179
Diagonal	d_1	79.67 - 100.32	161.67 - 179
Diagonal	d_2	73.2 - 106.79	260 - 270

The surface of the beam shell can be conveniently represented in θ - z plane, where (r, θ, z) are cylindrical coordinates, or alternatively, in the p - z plane, where p is the arc-length coordinate at the outer edge of the shell:

$$p(\theta)=\int_{\theta_0}^{\theta}\left[\left(\frac{\mathrm{d}r}{\mathrm{d}\theta}\right)^2+r^2\right]^{1/2}\mathrm{d}\theta \tag{1}$$

where $r^2 = x^2 + y^2$, and $x = a_{maj}\cos\theta$, $y = a_{min}\sin\theta$, and a_{maj} = 100 mm, a_{min} = 60 mm. The representation θ - z was used for visualization, since the association with the angle θ is more intuitive, whereas p - z was used for the length and orientation assessment. All faults on the test object were designed to be crack-like and were placed on the upper half of the beam. The dimensions of the damage feature were fixed for all simulations, with a crack of Δl = 20 mm, width = 1 mm, and a depth of 2mm. The positions (Fig. 2) of the different crack-type faults analyzed in this work with respect to the θ and z coordinates are given in Table 4. The faults d_1 and d_2 are diagonal damages with inclinations of 60° and 30° with respect to the z coordinate.

4. Damage Detection

4.1 Metrics used in this work

Coordinate Modal Assurance Criterion

The Coordinate Modal Assurance Criterion (COMAC) is an extension of the Modal Assurance Criterion (MAC) [7], seeking to identify which measurement point contributes negatively to a low MAC value. This criterion is calculated based on the healthy and damaged mode shapes by means of the following formula [8]:

$$\mathrm{COMAC}(i,j)=\frac{\left(\sum_{r=1}^{N}\left|\varphi_r^{(u)}(i,j)\varphi_r^{(d)}(i,j)\right|\right)^2}{\sum_{r=1}^{N}\left(\varphi_r^{(u)}(i,j)\right)^2\sum_{r=1}^{N}\left(\varphi_r^{(d)}(i,j)\right)^2} \tag{2}$$

where N is the number of mode shapes and $\varphi_r^{(u)}(i, j)$ and $\varphi_r^{(d)}(i, j)$ are the values of the nodal displacement at nodes (i, j) in the rth mode of the undamaged (u) and damaged (d) structure, respectively. By definition, COMAC is a dimensionless quantity contained in the interval [0,1], where a value of 0 implies no correlation (pointing to damage near the node) while a value of 1 implies full correlation (no damage near the node) [19]. In this paper, COMAC was calculated with the first 10 displacement modes obtained with the finite-element model built in ANSYS.

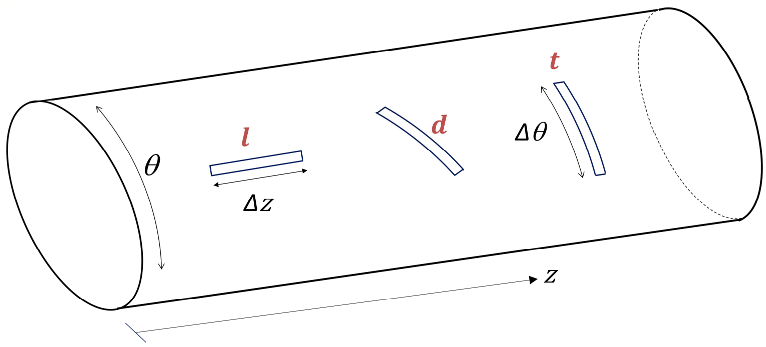

Fig. 2. Geometry of the test object and nomenclature of the damage features studied.

Mode shape differences

The mode shape difference (MSD) is the value obtained when the mode shape of the damaged structure is subtracted from the undamaged structure's mode shape [3]. To summarize the results for all modes, the average mode shape difference at a given node is calculated for all modes. As in the case of the COMAC metric, 10 displacement modes obtained with ANSYS were used to create MSD damage maps:

$$\mathrm{MSD} = \sum_{r=1}^{N} \frac{\varphi_r^{(u)}(i,j) - \varphi_r^{(d)}(i,j)}{N} \tag{3}$$

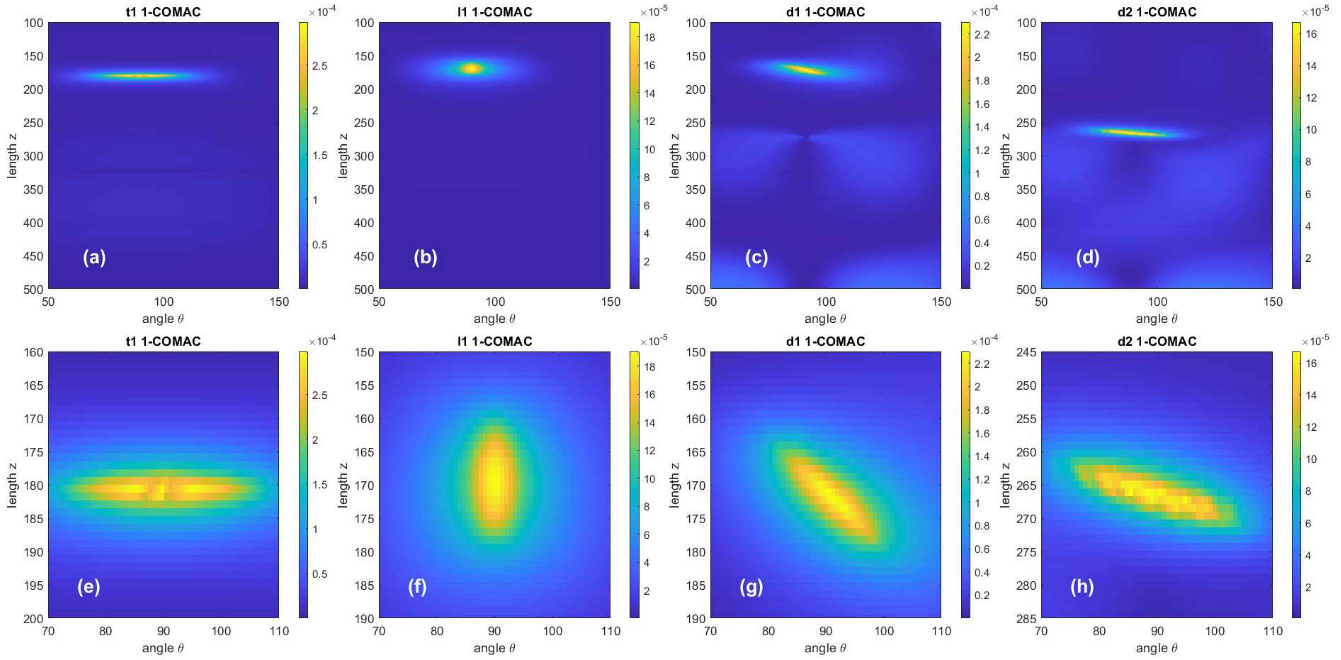

Fig. 3. Damage maps in the θ - z plane of the sample, obtained with the COMAC metric for all four damage features studied in this work for the case of vanishing noise. Upper row (subplots (a)-(d)): Overview of the upper surface of the sample. Lower row (subplots (e)-(h)): close-ups of the damaged regions. First column (plots (a) and (e)): transverse fault t_1. Second column ((b) and (f)): longitudinal fault l_1. Third column ((c) and (g)): diagonal fault d_1 oriented at 30° with respect to the z-axis. Fourth column ((d) and (h)): diagonal fault d_2, oriented at 60° with respect to the z-axis.

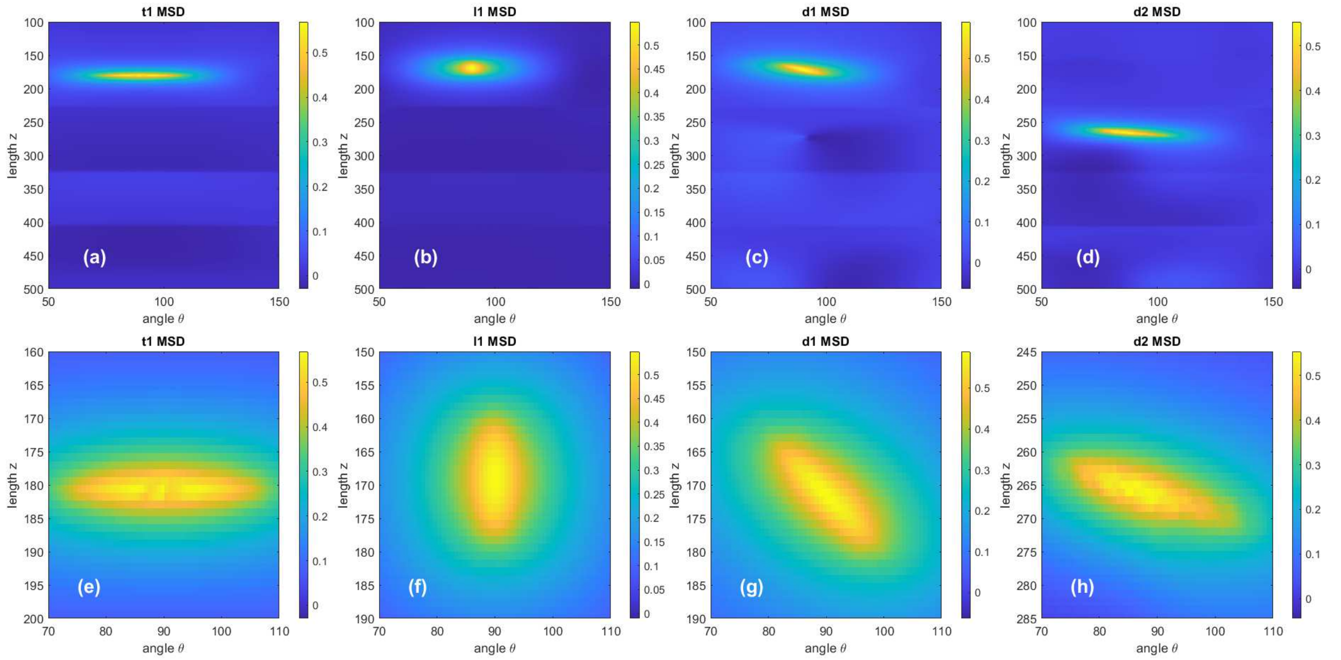

Fig. 4. Damage maps in the θ - z plane of the sample, obtained with the MSD metric for all four damage features studied in this work for the case of vanishing noise. Upper row (subplots (a)-(d)): Overview of the upper surface of the sample. Lower row (subplots (e)-(h)): close-ups of the damaged regions. First column (plots (a) and (e)): transverse fault t_1. Second column ((b) and (f)): longitudinal fault l_1. Third column ((c) and (g)): diagonal fault d_1 oriented at 30° with respect to the z-axis. Fourth column ((d) and (h)): diagonal fault d_2, oriented at 60° with respect to the z-axis.

4.2 Damage detection in the absence of noise

Damage detection with the COMAC and the MSD metric

As an introduction to the damage assessment, damage maps obtained with the COMAC and MSD methods will be shown for the case of vanishing noise. Figure 3 shows the damage maps obtained with COMAC for all four faults studied in this work: transverse (t_1), longitudinal (l_1), and diagonal (d_1 and d_2). The damage features can clearly be distinguished as elliptical features in the (θ, z)-plane of the sample, with the orientations and major axes of the ellipses being roughly consistent with the angles and lengths of the cracks, as confirmed by the close-ups into the damage regions (subplots (e)-(h)).

Similar results have been obtained with the MSD metric, as evidenced by Figure 4. The overall conclusions are the same as for the COMAC case. The damage signal appears to stand out somewhat more compared to the COMAC case; otherwise, the results appear to be very similar.

4.3 Damage detection with finite noise levels

Damage maps at different SNR levels

In practice, the presence of noise is inevitable. Therefore, it is important to assess the robustness of the methods in the presence of noise. For the analysis of the signals with noise, Gaussian white noise was introduced to the information of the mode shapes, obtained with ANSYS. For this, the MATLAB awgn command was used, for which it is necessary to specify the SNR signal to noise ratio. The signal-to-noise-ratio (SNR) is expressed as [17]:

$$\mathrm{SNR} = 10\log_{10}\left(\frac{P_{\mathrm{signal}}}{P_{\mathrm{noise}}}\right) = 20\log_{10}\left(\frac{1}{e}\right) \tag{4}$$

where P denotes the average power of the signal and e is the noise level. The different damages were analyzed under different noise levels. Figure 5 shows damage maps at finite noise levels, obtained with the MSD (subplots (a, c)) and the COMAC method (subplots (b, d)), respectively. In can be seen that neither of the methods MSD method is capable of detecting the location of the damage by itself for SNR levels smaller than 40 dB.

Wavelet de-noising

Wavelet transform has been extensively used for signal de-noising [20]; [21]; [22]. The basic idea behind the wavelet-based de-noising is to decompose the original signal into multiple sub-bands of wavelet coefficients at the chosen level [17]. In the present context, a noisy damage map (obtained with either the MSD or the COMAC method) s_n can be represented by:

$$s_n(i,j) = s_0(i,j) + \sigma e(i,j) \tag{5}$$

where s_0 (i, j) is a MSD or COMAC map derived from the two-dimensional modes shapes calculated with the FE model. finite-element, and e is the noise signal with variance σ^2. In this work, the Matlab command s_n = awgn(s_0 (i, j), SNR) was used to add Gaussian noise to the original signal at a given SNR ratio. The *de-noising* procedure consists of three steps: (1) wavelet decomposition, (2) specification and application of a threshold to the wavelet detail coefficients, and (3) reconstruction of the signal by using only detail coefficients above the threshold. In the first step, a wavelet type is chosen and the number of decomposition levels L is specified according to

$$L = \mathrm{floor}(\log_2 N) \tag{6}$$

where N is the number of samples in the data set. The wavelet decomposition of the signal is conducted down to level L. In the second step, the detail coefficients are subjected to threshold filtering using

$$\mathrm{Threshold} = \sqrt{2\ln\left(\mathrm{length}\left(s_{n,j}\right)\right)} \tag{7}$$

as a threshold. The expression of eq. (7) is also referred to as the *universal threshold*. $s_{n,j}$ identify the columns of the matrix s_n (i, j). In the final step, the signal is reconstructed using the estimated wavelet detail coefficients [20]. In this paper, the Matlab command wdenoise was used for this process, in conjunction with the wavelet Symlet4.

It should be pointed out that the (discrete) wavelet-based de-noising process described above is completely different from the two-dimensional Continuous Wavelet Transform process and should not be confused with the latter.

Damage location with wavelet de-noising

An example of the usefulness and limitations of the wavelet de-noising process described in the previous subsection will be discussed below. Fig. 6 shows the results of the de-noised MSD damage maps for different signal-to-noise ratios (SNR = 65, 40, 28, and 14 dB). The specific values chosen correspond to some of the values reported in literature as the SNR levels required for a correct detection of a damage feature; see Table 2. As can be seen from Fig. 6, de-noising alone provides good results at generous SNR levels such as 65 dB or 40 dB, where the original damage signal can be reconstructed very well. At SNR = 25 dB, it is still possible to discern a signal, but the shape is totally distorted and any prospect of detecting geometric features of the fault appears to be unlikely. At still lower levels, such as SNR = 14 dB (Fig. 6 (d)), the signal barely stands out of the noise background.

Two-dimensional Continuous Wavelet Transform (2D-CWT)

The continuous wavelet transform (CWT) of a one-dimensional signal f (x) is given by:

$$Wf(u,s) = \langle f, \psi_{u,s} \rangle = \frac{1}{\sqrt{s}} \int_{-\infty}^{\infty} \left\langle f(x),\, \psi\left(\frac{x-u}{s}\right)\right\rangle dx \tag{8}$$

where $Wf(u,s)$ is the wavelet coefficient for the family of wavelets $\psi_{u,s}$. u and s are the translation and scale parameter, respectively. The function ψ is generally referred to as the *mother wavelet*. The set of functions ψ ((x–u)/s) is the corresponding *wavelet family,* derived from the mother wavelet. The 1-D wavelet transform can be extended to 2D, as described in the following. Let $f(x,y)$ be a signal belonging to the Hilbert space $L^2(R^2)$. The horizontal wavelet $\psi^{(1)}(x, y)$ and its vertical counterpart $\psi^{(2)}(x, y)$ can then be constructed from separable products of a scaling function φ and a wavelet function ψ:

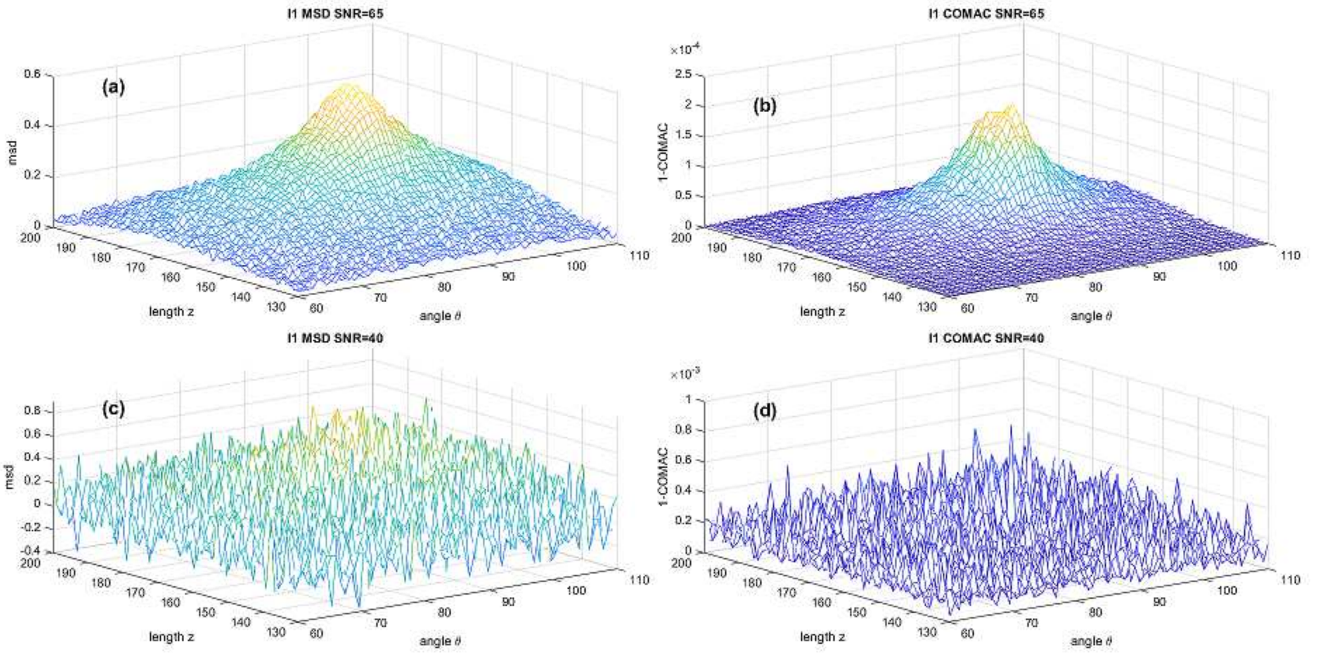

Fig. 5 Damage maps in the θ - z plane for the longitudinal crack l_1 for two SNR levels (65 dB) and 40dB). *Left* (subplots (a) and (c)): MSD method. *Right* (subplots (b) and (d)): COMAC method.

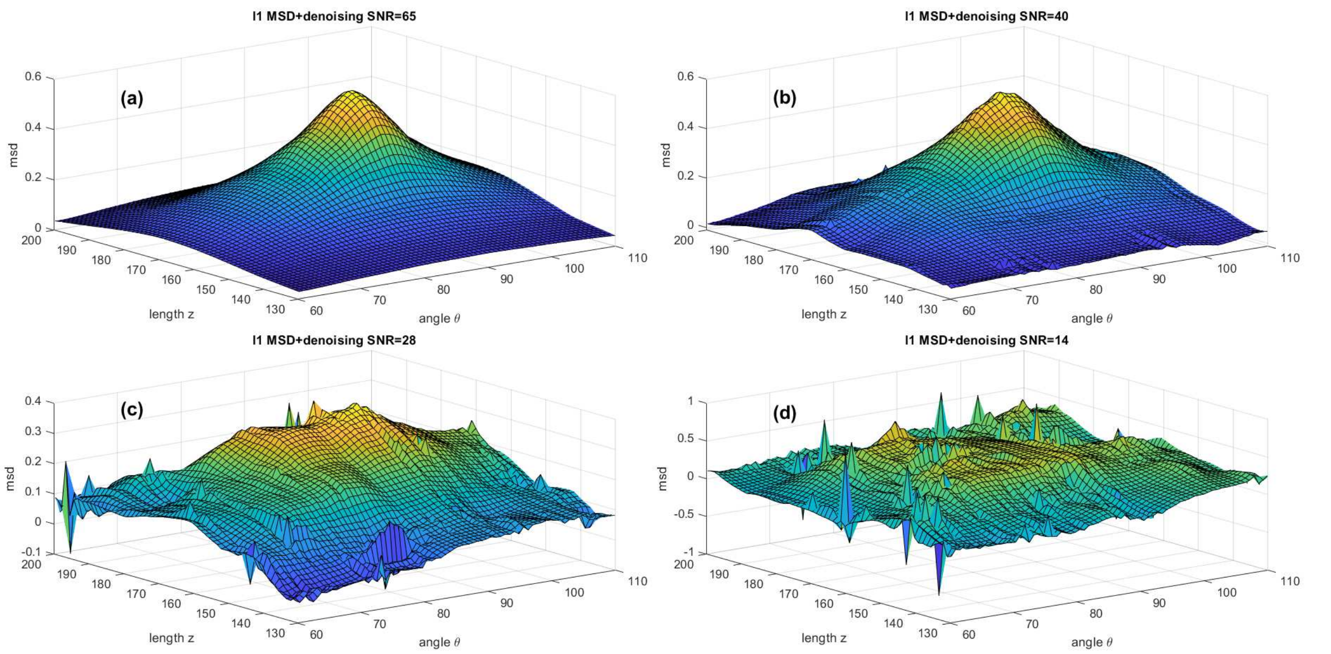

Fig. 6. The effect of wavelet de-noising on MSD damage maps for the longitudinal crack l_1, shown for four SNR levels. (a) 65 dB, (b) 40 dB, (c) 28 dB, and (d) 14 dB.

$$\psi^{(1)}(x,y) = \varphi(x)\psi(y) \tag{9}$$

$$\psi^{(2)}(x,y) = \psi(x)\varphi(y) \tag{10}$$

A family of wavelet functions can then be defined as follows:

$$\psi_{u,v,s}^{(i)} = \frac{1}{s}\psi^{(i)}\left(\frac{x-u}{s},\frac{y-v}{s}\right), i = 1,2 \tag{11}$$

The 2-D continuous wavelet transform of the function $f(x, y)$ defined with respect to vertical and horizontal wavelets, can then be defined as [23]:

$$W^{(i)}f(u,v,s) = f,\psi_{u,v,s}^{(i)} = \frac{1}{\sqrt{s}}\int_{-\infty}^{\infty}\int_{-\infty}^{\infty} f(x,y)\psi^{(i)}\left(\frac{x-u}{s},\frac{y-v}{s}\right)\mathrm{d}x\mathrm{d}y \tag{12}$$

A sudden peak in the wavelet coefficient analyzed indicates a candidate location for damage in the structure. In this work, the function $f(x, y)$ represents a given mode shape of the TWCB test sample, obtained with the finite-element model.

Mother wavelet

No fixed rules exist for the selection of a mother wavelet, so the most appropriate mother wavelet generally depends on the type of problem [24], and trial-and-error approaches are often applied to choose the most appropriate mother wavelet [25]. Different mother wavelets have been used for damage detection with the two-dimensional wavelet transform, such as the Haar wavelet [17], the Paul wavelet [4], the Derivative of the Gaussian (DoG) wavelet [26], and the Gabor wavelet [19]. In this work, the Derivative of the Gaussian wavelet was used. The DoG wavelet is given by [26]:

$$\psi_{\mathrm{DoG}}(X) = \nabla^2 G(X) = \frac{r^2 - \sigma^2}{\sigma^4} \exp\left(-\frac{X^2}{2\sigma^2}\right) \tag{13}$$

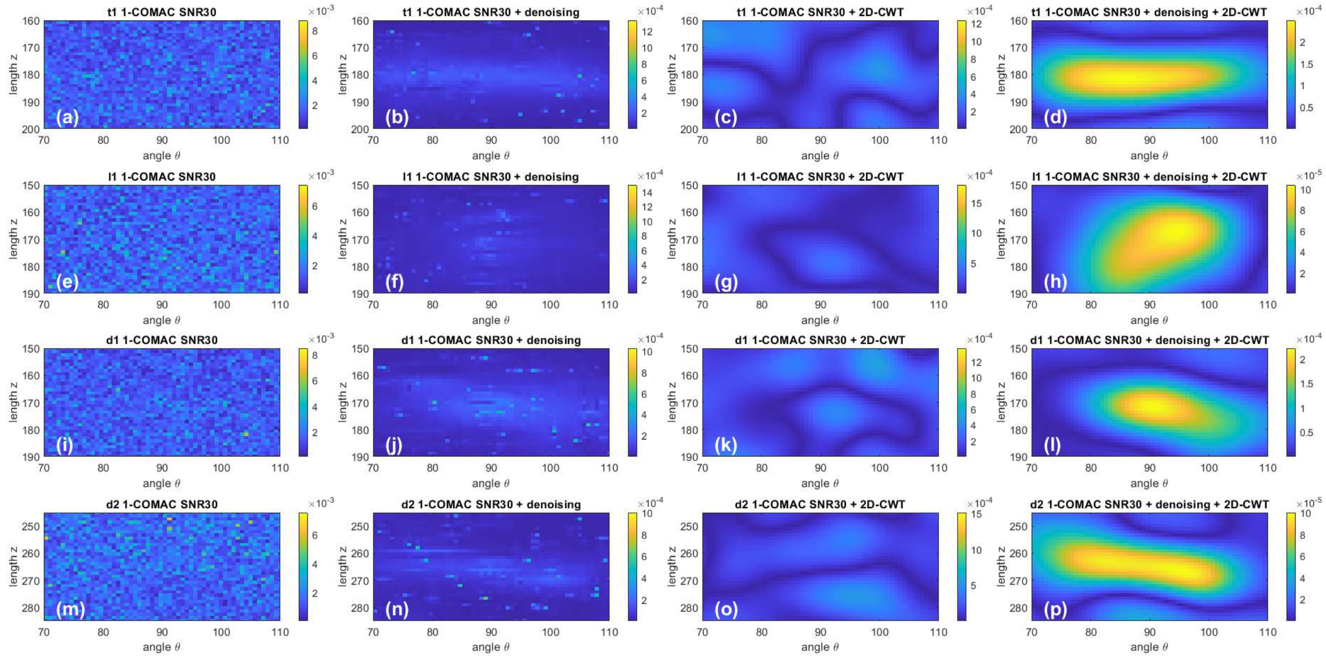

Fig. 7. Effect of the different processing steps implemented in this work for the case of the COMAC method. *Rows*: fault type (transverse, longitudinal, diagonal 30°, diagonal 60°). *Columns*: Processing method (none, de-noising only, 2D-CWT only, de-noising + 2D-CWT). SNR = 30 and *s* = 6 in all cases.

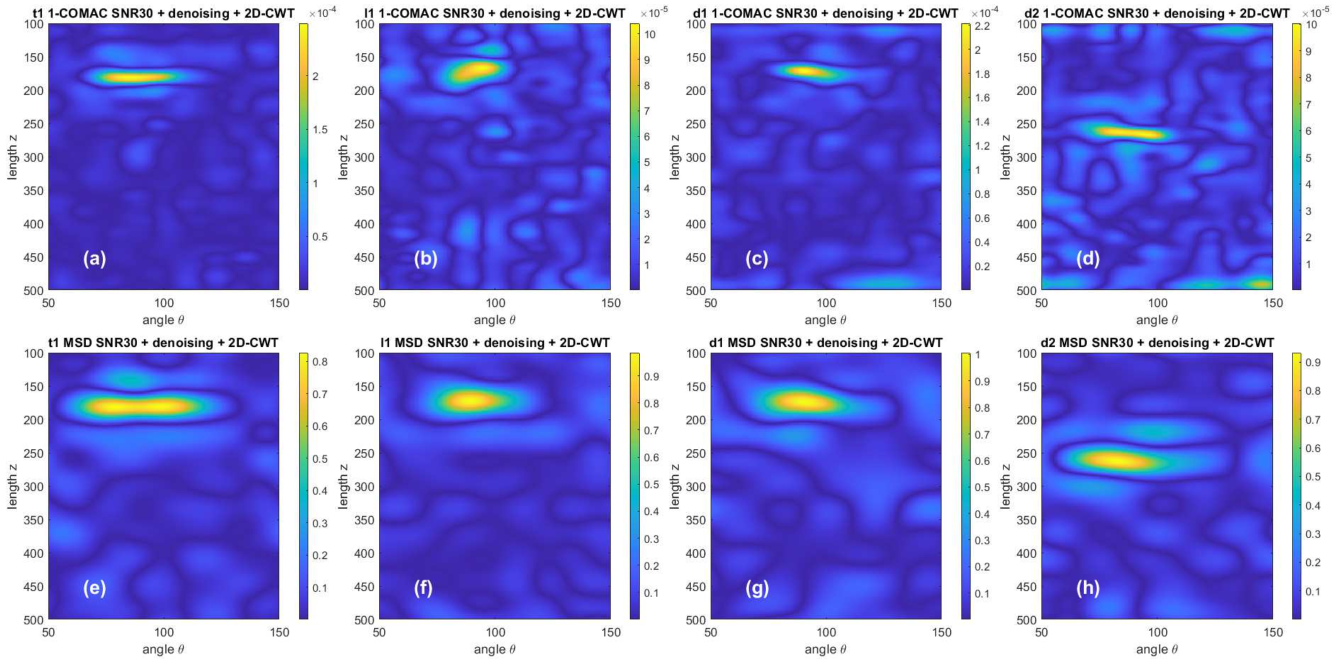

Fig. 8. 2D-wavelet transformed COMAC (top row) and MSD (bottom row) damage maps all four cracks (transverse t_1, longitudinal l_1, diagonal d_1, diagonal d_2), with de-noising conducted prior to the 2D-wavelet transform. The signal-to-noise ratio (SNR) was 30 in all cases *s* = 6.

Damage location with and de-noising and 2D-CWT

As mentioned before, damage detection and location is achieved through a combination of (wavelet) de-noising and a 2D Continuous Wavelet Transform (CWT), as shown in Fig. 1. The effect of the different processing steps is illustrated in Fig. 7 for the case of the COMAC metric. Damage maps pertaining to a given row pertain to a particular type of fault (transverse, longitudinal, diagonal 30°, diagonal 60°), whereas columns show the effect of a specific combination of processing steps (none, de-noising only, 2D-CWT only, de-noising + 2D-CWT). It can be seen that even at a generous signal-to-noise ratio of SNR = 30 no hint of a damage feature shows up in the damage map (first column). De-noising (second column) evidently reduces the noise level, but only a very faint hint at the faults appears, which can hardly be distinguished from the background. The direct application of the 2D-CWT method produces certain structures, but those do not align with the true fault positions, extensions and orientations. The combined application of de-noising and 2D-CWT, finally, (fourth column) does produce a clear signal in the θ - z plane (yellow areas), which can be further analyzed for their usefulness for damage assessment. DoG mother wavelet and a scale of s = 6 were used for all DWT-processed maps.

A comparison of the COMAC and the MSD method is shown in Fig. 8, where the wavelet coefficients obtained from de-noised versions of the COMAC and MSD damage maps have been dispalyed again using a DoG mother wavelet and a scale of s = 6. It can be seen that the intensity of the damage signal is about the same in both methods, with the COMAC method producing a somewhat narrower signal. Either methods seem to be suitable for damage *detection*, though it is not clear at this point whether these approaches are also useful for a *quantitative assessment* of the damage. As will be shown below, this is indeed the case.

5. Length and Orientation Assessment

While detecting and locating a fault in a structure, possibly in combination with a certain threshold for the damage intensity, may sometimes be enough to trigger a certain action, e.g. an inspection followed by a corrective maintenance procedure, often it may be critical to also know the *size* of the fault. It may be possible to tolerate an incipient crack for a certain amount of time, especially if the inspection and maintenance procedure is costly (involving, say, a helicopter flight to an off-shore wind farm), whereas a crack of a certain length might trigger immediate action (say, curtailing or shutting down a wind turbine). Measuring the length of a crack therefore adds significant value to a Structural Health Monitoring (SHM) approach. The orientation of a crack also provides additional useful information, as it may provide tale-tell evidence of the nature of the fault.

The general idea used in this work starts with the observation that crack-type faults translate into features in the processed damage maps which can be well approximated by continuous two-dimensional functions fit (x, y). Ideal damage maps (either MSD or COMAC), obtained in the absence of noise, and without further processing yield damage features with can almost perfectly been fitted with bi-normal functions. Though the presence of noise precludes the direct use of MSD or COMAC maps, as explained above and shown in Fig. 7, the processed maps (after applying a de-noising and a 2D-CWT stage) still produce damage features which are roughly bi-normal. The key question arising is then evidently: are the scale parameters of the bi-normal fit consistent with the length and orientation of a given crack? In other words, can the geometrical parameters of the crack be *measured* with this method? As it will be shown below, the answer to this question is yes.

5.1 Length measurement of crack-type faults: general approach

For the evaluation of the damage size, a bi-normal function surface fitting procedure is performed on the results on the CWT surfaces obtained from de-noised MSD or COMAC maps. A bi-normal function has the following structure:

$$\mathrm{fit} = A\exp\left(-\left(\frac{p-b}{c}\right)^2 + g\frac{(p-b)(z-e)}{-d} + \left(\frac{z-e}{f}\right)^2\right) \tag{14}$$

where A is an overall amplitude, (b, e) is the center location of the fault, and (c, f) are characteristic spreads of the fault in the p and z direction, respectively. For convenience, the “toggle” parameter g has been introduced, indicating whether the bi-normal bell curve is oriented along either of the two axes p or z, in which case g = 0, or whether the more general case of an arbitrary orientation applies (g = 1). The parameter d controls the rotation angle of the function.

5.2 Length measurement at transverse and longitudinal cracks

It is instructive to first study the case of transverse (z = const.) or longitudinal (p = const) cracks. In this case, the toggle parameter g is equal to zero. A few illustrative results have been plotted in Figure 9, where a section of the de-noised and CWT-transformed MSD map in the vicinity of the longitudinal crack has been plotted for different signal-to-noise ratios (SNRs = 65, 40, 28, and 14 dB) and a scale value of 12, together with the best bi-normal surface fits. The fit function is shown in intense colors, whereas the empirical data have been plotted as a mesh plot (light colors). It can be seen that the fit is fairly good in all cases. A somewhat more conspicuous deviation between the two surfaces arises at the base of the hill, where the empirical data set shows some oscillations, resulting from the CW transform, which mistakenly interprets some random fluctuations as structural features; see also Figure 8 and the corresponding interpretation.

The next question arising is how to interpret the scale parameters of the bi-normal surface plot. It can be seen from Fig. 9 that the fit surface has a finite extension in both the longitudinal (z) and transverse (p) direction, so it is not clear from the outset what the predominant crack orientation should be. The following three-part hypothesis was established and tested: (1) The width of the crack cannot be resolved with the method proposed in this work, at least not under realistic noise levels. (2) The dimension associated with the crack orientation is the one with the larger characteristic scale (c or f, respectively). (3) The characteristic dimension in the crack direction is a well-defined measure of the crack length. Part 1 of the hypothesis is due to the recognition that even a very small crack width (1mm, in this case) produces a relatively spread of the damage signal in that direction (albeit smaller than in the crack direction). Part 2 states the (expected) observation that the signal spread in the crack direction (if measured in the p-z plane) is larger than the spread in the perpendicular direction, thereby also allowing to determine the orientation of the crack; see below for a more systematic approach to this subject. Part 3, finally, expresses the expectation that a systematic relationship should exist between the crack length and the characteristic scale, at least for a given combination of detection method (MSD or COMAC) and scale factor, and that a method could be devised for inferring the true length from a set of measurements or processing steps.

Exploring the validity of the above assumptions we will first refer to the case of the longitudinal fault l_1. To quantify the results, the length ratio $r_l = \Delta l/f$ has been defined, measuring the ratio between the true fault length Δl and the characteristic scale f of the bi-normal fit for the z-direction. Similarly, a length ratio for transverse faults can be defined by $r_t = \Delta l/c$. The general case of arbitrarily oriented crack will be discussed further below.

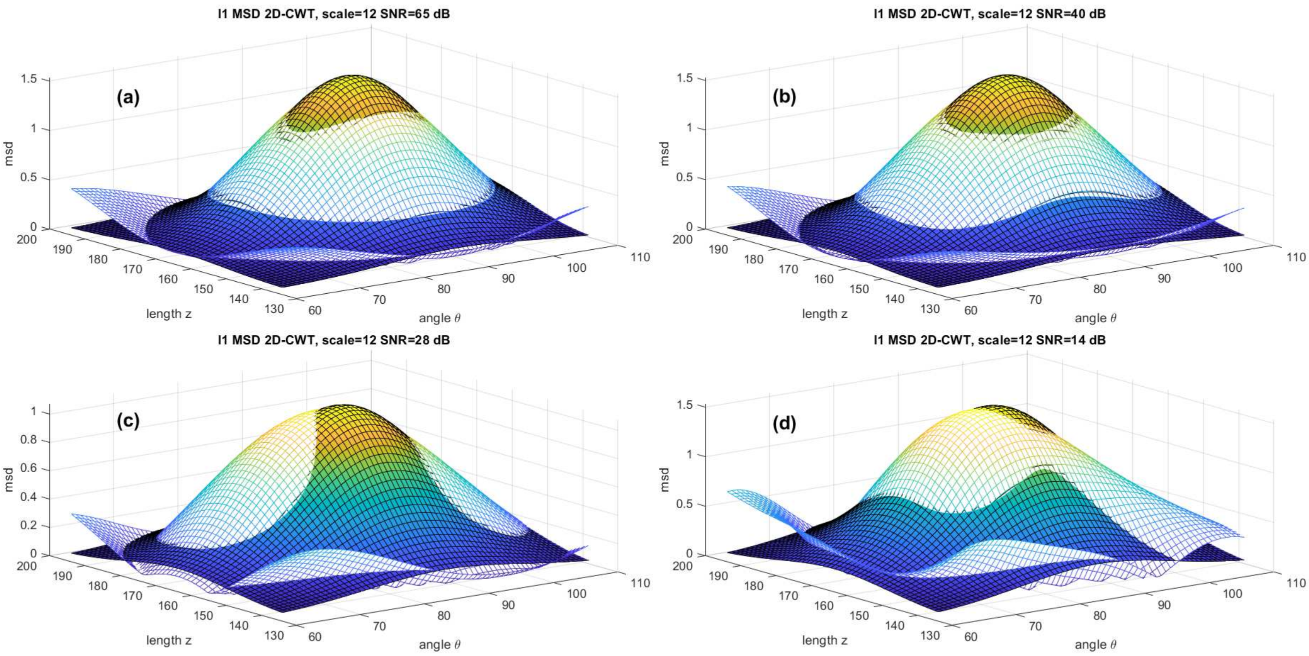

Fig. 9. Example results of the bi-dimensional curve fitting process, shown for the case of the longitudinal crack and the MSD method. (a) SNR = 65dB, (b) 40dB, (c) 28dB, (d). The scale parameter of the 2D-CWT was s = 12 in all cases.

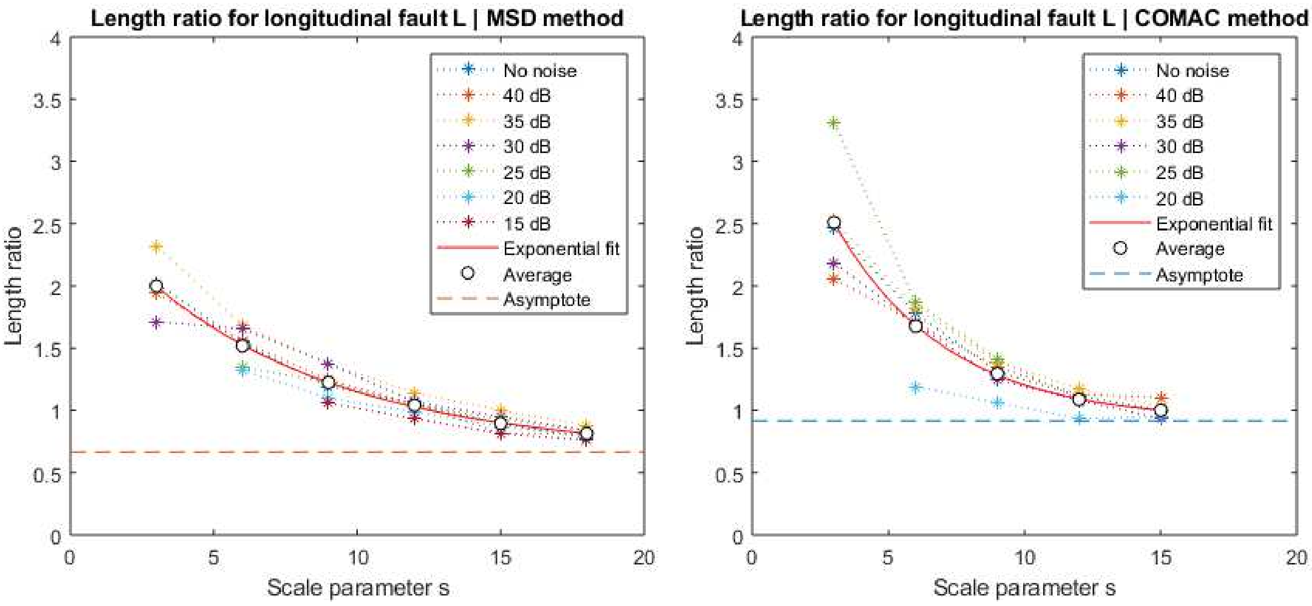

Fig. 10. Measurement of the length of the longitudinal fault with the MSD (left) and the COMAC method (right) as a function of the scale parameter and for different noise levels. Both graphs show the longitudinal length ratio r_l.

The results for the longitudinal length ratio as a function of both the signal-to-noise ratio and the 2D-CWT scale factor, r (s, SNR_i), are shown in Fig. 10, with the left plot corresponding to MSD and the right plot to the COMAC method. As expected, the use of larger CWT scale factors s lead to larger characteristic lengths of the damage feature in MSD and COMAC maps; consequently, r decays monotonically with s The noise level, o equivalently, the SNR level has some influence on the results, but the influence is minor, with the possible exception of a few data points in the COMAC case. As shown in Fig. 10, the average r curve, $\langle r\rangle(s) = \Sigma\, r\,(s, SNR_i) / N_{SNR}$, with $N_{SNR} = 5$ being the number of SNR levels, can be fitted almost perfectly to an exponential curve of the form

$$r_{\rm fit} = r_\infty + \Delta r \exp(-s/s_c) \tag{15}$$

This holds true in both cases, i.e. using either the MSD or the COMAC method, though with different fit parameters. In the case of the transverse length ratio, the r_t (s, SNR_i) curves for individual signal-to-noise ratios SNR_i show a slightly more complex behavior than in the previous case of longitudinal faults, but the overall variation is smaller. The average r_t curves $\langle r_t\rangle(s) = \Sigma\, r_t\,(s, SNR_i) / N_{SNR}$ are much flatter than in the longitudinal case, reaching a near-asymptotical value for scale factors s of the order of 6. As before, the exponential fit (eq. (13)) represents a very good approximation to the average curve. As shown below, this trend continues to hold in the more general case of diagonally oriented faults. This case will be described next.

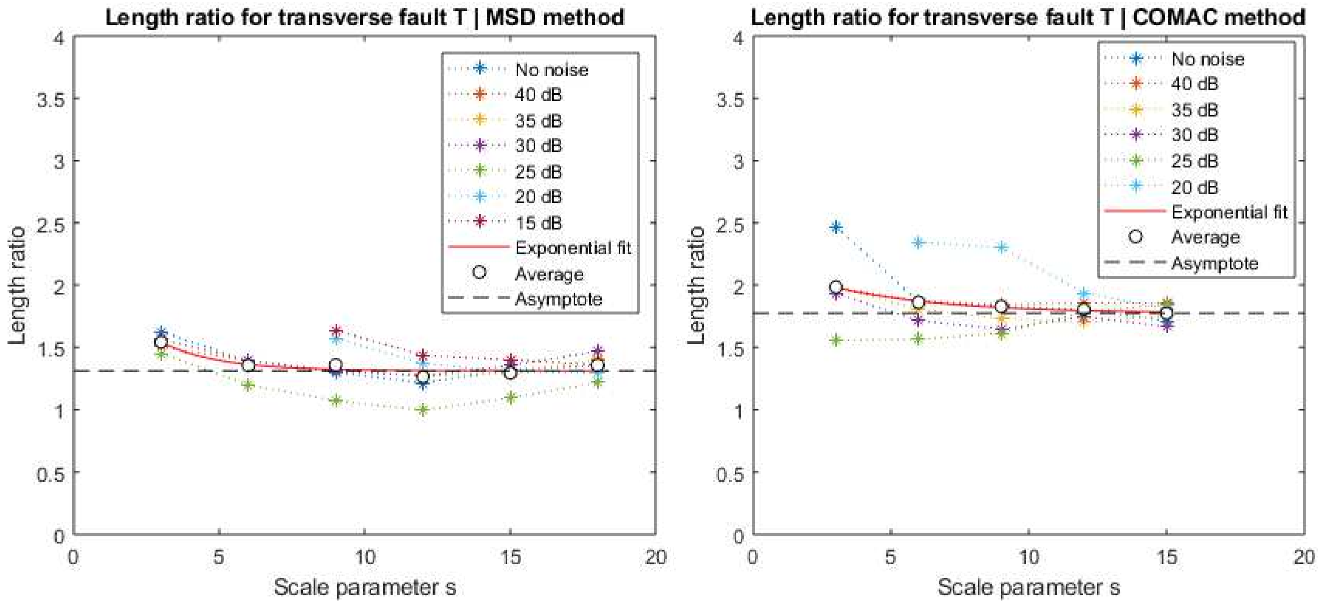

Fig. 11. Measurement of the length of the transverse fault with the MSD (left) and the COMAC method (right) as a function of the scale parameter and for different noise levels. Both graphs show the transverse length ratio r_t.

5.3 Length measurement at diagonal cracks

Diagonal cracks correspond to the general case of the bi-normal fit, where the toggle parameter g has been set to $g = 1$. In this case, the argument of the exponential function in eq. (12) can be written as

$$\arg(\text{fit}) = [X \quad Y]\begin{bmatrix} \frac{1}{c^2} & -\frac{2}{d} \\ -\frac{2}{d} & \frac{1}{f^2} \end{bmatrix}\begin{bmatrix} X \\ Y \end{bmatrix} = [X \quad Y]\mathbf{A}\begin{bmatrix} X \\ Y \end{bmatrix}, \tag{16}$$

where $X = p - b$ and $Y = z - e$. $\mathbf{A}$ is the symmetric matrix that characterizes the quadratic form. Given its symmetry, $\mathbf{A}$ is orthogonally diagonalizable, i.e. $\mathbf{Q}^T\mathbf{A}\mathbf{Q} = \mathbf{Q}^{-1}\mathbf{A}\mathbf{Q} = \mathbf{D}$, where $\mathbf{D}$ is a diagonal matrix. The matrix $\mathbf{Q}$ is obtained with the normalized eigenvectors:

$$Q = (\tilde{\upsilon}_1, \tilde{\upsilon}_2) \tag{17}$$

$$\begin{bmatrix} X_a \\ Y_a \end{bmatrix} = Q\begin{bmatrix} X_a' \\ Y_a' \end{bmatrix} \Rightarrow [X_a \quad Y_a] = [X_a' \quad Y_a']Q^T \tag{18}$$

Consequently,

$$\arg(\text{fit}) = [X_a' \quad Y_a']\begin{bmatrix} \lambda_1 & 0 \\ 0 & \lambda_2 \end{bmatrix}\begin{bmatrix} X_a' \\ Y_a' \end{bmatrix} = [X_a' \quad Y_a']\mathbf{D}\begin{bmatrix} X_a' \\ Y_a' \end{bmatrix} \tag{19}$$

where $\lambda_{1,2}$ are the eigenvalues of $\mathbf{A}$. Given that the representation of arg(fit) in eq. (15), for the general case $g = 1$, is completely analogous to the special $g = 0$. the measurement of the crack length can also proceed in a similar way. Now that arg(fit) with $g = 1$ has been cast into a form analogous to the special case $g = 0$, the characteristic scale in the direction of the crack can be obtained from:

$$l_{\text{crack}} = \sqrt{\frac{1}{\min(\lambda_1, \lambda_2)}} \tag{20}$$

Defining a length ratio as before, now for diagonal (i.e., arbitrarily oriented cracks), by $r_{\text{diag}} = \Delta l / l_{\text{crack}}$, where the true crack length continues to be $\Delta l = 20$ mm, we can now study r_{diag} (s, SNR). The results are shown in Figures 12 and 13.

It is conspicuous from both figures that the general observations obtained with the transverse and longitudinal fault, respectively, still hold in these more general cases. As before, the dependence of r_{diag} (s, SNR) on SNR is minor, with the main trend being determined by the dependence on the scale factor. A possible exception is the case of the three lowest SNR values (15, 20, and 25 dB) in the case of the MSD method, which seem to have a systematically lower length ratio as the damage features at higher signal-to-noise ratios. This result has of course to be taken with a grain of salt, as more in-depth analyses with better statistics (which are beyond the scope of the present work) might reveal this difference to be a statistical fluctuation. In any case, in order to err on the safe side, a separate average and fit curve have been calculated for these three low-SNR cases; see Fig. 11. It is conspicuous that even in these cases the asymptotic length ratio r_∞ seems to be approximately the same, making r_∞ a candidate for a robust measure of the crack length.

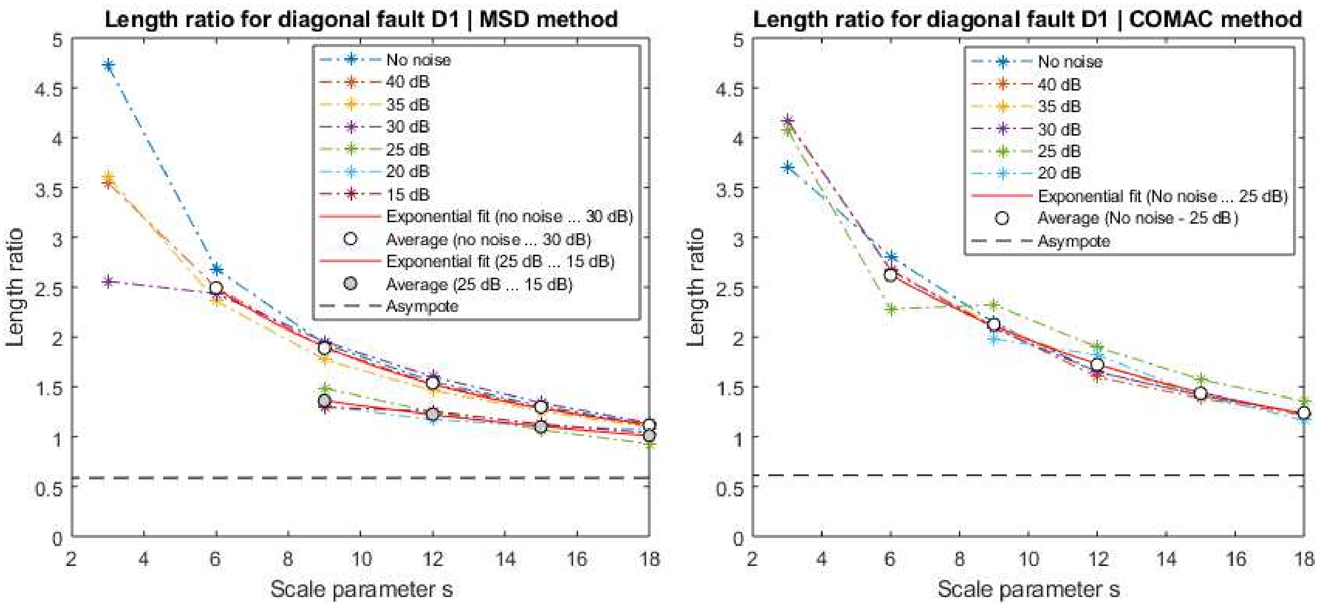

Fig. 12. Measurement of the length of the diagonal fault d_1 with the MSD (left) and the COMAC method (right) as a function of the scale parameter and for different noise levels. Both graphs show the diagonal (general) length ratio r_{diag}.

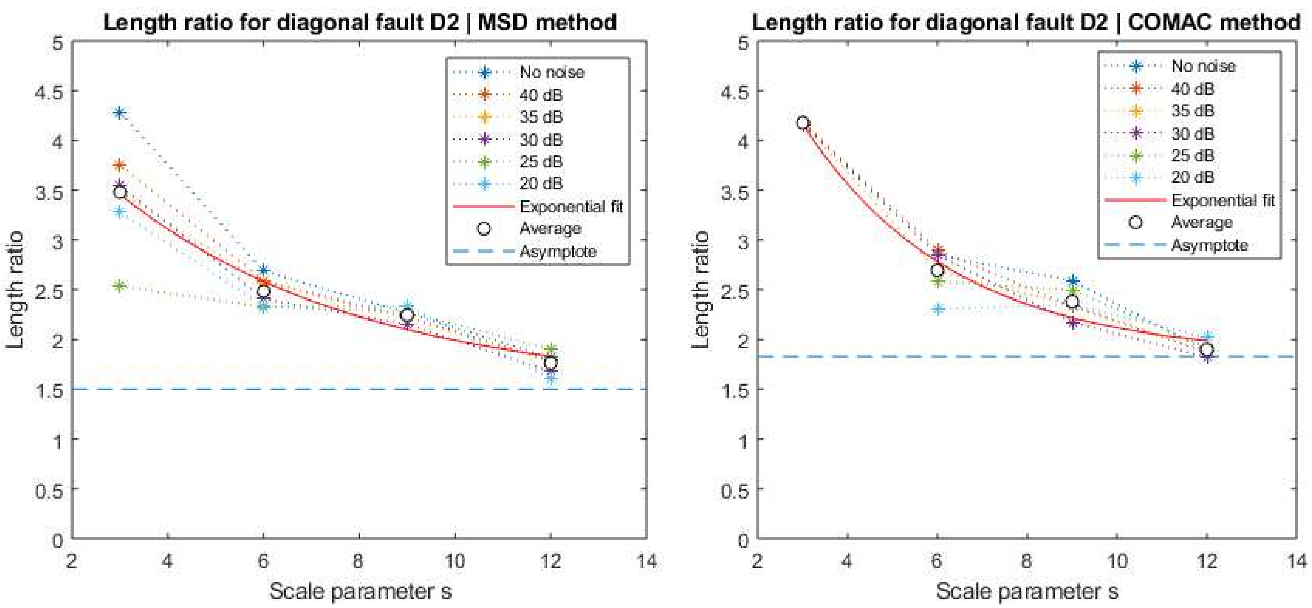

Fig. 13. Measurement of the length of the diagonal fault d_2 with the MSD (left) and the COMAC method (right) as a function of the scale parameter and for different noise levels. Both graphs show the diagonal (general) length ratio r_{diag}.

Table 5. Predicted crack angles in degrees (°) for the transverse fault, with nominal crack angle of 0°, using the MSD (left) and COMAC method (right), respectively.

	MSD-predicted angle							COMAC-predicted angle					
	SNR level							SNR level					
Scale	Inf	40	35	30	25	20	15	Inf	40	35	30	25	20
3	0.12	0.05	7.04	0.04	0.06			2.58	2.62	2.55	2.38	2.88	
6	0.16	0.06	1.15	0.64	0.06			1.58	3.91	1.83	2.49	3.21	5.02
9	0.29	0.35	0.04	1.21	0.07	0.18	0.06	1.61	1.67	1.69	1.68	3.55	5.59
12	0.46	0.6	0.05	1.39	0.05	0.53	0.06	3	3.13	2.91	2.69	4.58	3.16
15	1.12	1.35	1.16	1.74	5.69	0.22	0.07	6.99	6.48	6.12	5.57	9.95	7.47
Med.	0.22							3					

5.4 Measuring the orientation of diagonal cracks

General approach

The method discussed in the preceding section, based on bi-normal fits, offers a natural option for determining the orientation of a crack. The key idea it to identify the crack direction with the principal axis of matrix **A** defined in eq. (14) associated with the smaller of the two eigenvalues. Assuming , the following expression for the predicted crack angle can be written:

$$\theta_{\text{crack}} = \arctan\left(\frac{v_2^{(\min)}}{v_1^{(\min)}}\right) = \theta_{\text{crack}}\left(c, d, f\right), \tag{21}$$

where $(v_1^{(\min)}, v_2^{(\min)})$ is the eigenvector of **A** corresponding to the smaller of the two eigenvalues.

Using this formulation, not only can predicted values for the crack direction in the cases of the diagonal faults d_1 and d_2 be calculated, but also can the predicted angles for the cases of the transverse and the longitudinal fault be verified, previously assumed to be 0° and 90°, respectively, by setting the toggle parameter g to zero. The calculations have been carried out for the SNR and scale parameter ranges as studied before, i.e. SNR $\in \{15,20,25,30,35,40\}$ dB and $s \in \{6,9,12,15,18\}$ and for both the MSD and the COMAC method. The results are shown below in Tables 5-8.

From the tables, a few observations can be made: (1) In general, the crack angle is well predicted; using the median of all measurements for a given angle and method as a quick indicator, it can be seen that the error is generally less than one degree, with the exception of the 60° case, where both MSD and COMAC err by about two degrees. (2) The MSD method appears to be providing somewhat more accurate estimates than COMAC, with the exception of the 60° case, where both methods perform similarly. (3) Neither the SNR level nor the scale factor appear to have a systematic impact on the results, except for the fact that in some of the cases (i.e. at very low SNR levels and large scale factors) no meaningful conversion of the fit method was obtained. Most of the variations observed appear to be related to statistical outliers, rather than systematic effects. A more in-depth study with larger statistics, outside the scope of the present work, should be able to clarify these aspects.

Statistical error assessment

It is fair to ask if the (small) discrepancies observed can be attributed to the statistical error associated with the bi-normal surface fitting process. From the outset, inspecting the discrepancies shown in Tables 5-8 it appears that the error is mostly marked by a systematic component, given the fact that is generally unipolar, with the exception of the 30° case, where bipolar errors have been observed. To assess the statistical error, the error propagating from the fitting process has been calculated by

$$\delta\theta_{\text{crack}} = \sqrt{\left(\frac{\partial\theta_{\text{crack}}}{\partial c}\delta c\right)^2 + \left(\frac{\partial\theta_{\text{crack}}}{\partial d}\delta d\right)^2 + \left(\frac{\partial\theta_{\text{crack}}}{\partial f}\delta f\right)^2}, \tag{22}$$

Table 6. Predicted crack angles in degrees (°) for the transverse fault, with nominal crack angle of 90°, using the MSD (left) and COMAC method (right), respectively.

	MSD-predicted angle							COMAC-predicted angle				
	SNR level							SNR level				
Scale	Inf	40	35	30	25	20	15	40	35	30	25	20
3	88.4	89.7	89.7	88.6				83.8	83.9			
6	89.5	89.4	89.4	89.6	89.5	87.4	89.1	83.9	84.1	83.4	84.5	83.9
9	89.7	89.7	89.4	85	89.5	86.2	89.9	82.7	84.1	83.9	83.7	83
12	89.8	87.7	89.7	89.4	89.8	89.8	90	85.4	86.4	84	83.9	85.2
15	89.9	85.8	89.7	89.5	84.3	89.7	89.9	84.5	84.5	82.8	83.9	86.9
18	89.7	85.1	89.7	89.2	82.7	89.3	89.9					
Med.	89.5							83.9				

Table 7. Predicted crack angles in degrees (°) for the diagonal fault d_1, with nominal crack angle of 60°, using the MSD (left) and COMAC method (right), respectively.

	MSD-predicted angle							COMAC-predicted angle					
	SNR level							SNR level					
Scale	Inf	40	35	30	25	20	15	Inf	40	35	30	25	20
3	62.1	62	62	62.2				62.4	62.3	62.3	62.3	62.3	
6	62.1	62.1	62.1	62.3				62.1	62.1	62.2	61.7	62.4	61.7
9	62	62.2	62.2	62.2	64.6	64.2	63.4	61.9	61.8	61.9	61.6	62.7	61.4
12	62	62.1	62.2	62	64.1	64.3	62.7	61.8	61.7	61.8	61.4	62.9	61.5
15	62	62.1	62.1	61.9	63.5	64.3	62.3	61.4	61.5	61.7	61.1	62.8	61.5
18	62.2	62.2	62.3	61.9	63	64.3	61.9						
Med.	62.2							61.8					

Table 8. Predicted crack angles in degrees (°) for the diagonal fault d_2, with nominal crack angle of 30°, using the MSD (left) and COMAC method (right), respectively.

	MSD-predicted angle						COMAC-predicted angle					
	SNR level						SNR level					
Scale	Inf	40	35	30	25	20	Inf	40	35	30	25	20
3	31.3	28.3	26.1	21.2	34.7	28.5	20.3	20.3	19.4	19.4		
6	31.2	29.5	28.6	29	30.8	30.5	30.7	29.8	32.9	29	35.4	29.5
9	31.5	30	29.1	30.8	32.6	31	35.6	35.7	33.7	31.1	34.7	28.3
12	34.6	33.2	32.4	34.6	34.8	39.8	35.2	36.6	31.3	36	34.1	36.7
Med.	30.9						32.1					

Table 9. Statistical errors (in degrees (°)) in the determination of the crack angle, propagating from the bi-normal fit, shown for the case of an angle of 30°.

	SNR level					
Scale	Inf	40	35	30	25	20
3	0.058	0.061	0.067	0.065	0.121	0.096
6	0.046	0.04	0.038	0.077	0.072	0.089
9	0.038	0.036	0.032	0.053	0.054	0.073
12	0.036	0.036	0.034	0.039	0.045	0.057

Table 10. Assessment of the systematic error in the determination of the crack angle, shown for the case of an angle of 30°, as a function of the processing stage

MSD / 30° crack angle	**Measured [°]**	**Abs. error [°]**
No processing	29.96	0.04
De-noising only	29.99	0.01
De-noising + 2D-CWT scale 3	31.52	1.52
De-noising + 2D-CWT scale 6	31.21	1.21
De-noising + 2D-CWT scale 9	31.49	1.49
De-noising + 2D-CWT scale 12	34.61	4.61

As can be seen in Table 9, the statistical errors in the crack angle determination, which can be attributed to the uncertainties and of the fit parameters, are generally small. Table 9 has the errors for the case of a 30° crack angle only, but the results are very similar for all other cases (not shown for brevity). Consequently, it can be concluded that the impact of the fitting procedure on the overall angle error is small.

Systematical error sources

In order to assess the impact of the processing steps on the prediction of the crack angle, the procedure described in this section has been applied to three types of damage maps: (1) The unprocessed damage, as provided by the MSD or COMAC metric, respectively. (2) The de-noised version of MSD or COMAC map. (3) The damage map, after being subjected to de-noising and 2D-CWT processing. In this case, different scale factors were explored as well. Evidently, damage detection through a direct application of the MSD or COMAC metric is possible only for very low noise levels, or equivalently, high SNR levels. Only in those cases can a meaningful comparison between unprocessed and processed damage maps be made.

Table 10 shows the results obtained for the case of the 30° crack, the MSD method, and a SNR level of 65 dB. It can be seen that under these near-ideal conditions the angle inferred with the methodology from the original MSD damage map is identical to the nominal value, within the statistical bounds given by the bi-normal surface fit; see Table 9. The de-noising step does not generate a significant change. The application of the 2D-CW transform, does, however, introduce a bias (of the order of 1.5°), which is roughly independent of the wavelet scale s (see also Table 7 for the case of the 60° crack angle). At the largest scale (s = 12) a somewhat higher bias is observed, which is not implausible, given that the size of the damage feature in CWT-transformed damage maps increases with scale, making the accurate determination of the angle potentially more difficult.

Given that the observed bias is larger for the diagonal cracks (~1.5 – 2.0°) compared to the cases where the crack is aligned with one of the coordinate axes (transverse and longitudinal faults, where the bias is a fraction of a degree), it cannot be ruled out that the choice of the coordinate system is important for the specific results obtained with the CWT transform. This hypothesis can of course be tested by using a coordinate system which is not aligned with the finite-element simulation mesh. In order to minimize the effect of the choice of the frame, CWTs conducted with different coordinates systems could be averaged, in order to obtain a consolidated result. Such sensitivity analyses are beyond the scope of the present work; the author do plan, however, on conducting such analyses in follow-up work.

Table 11. Fit parameters for the length ratio function r(s)

		Δr	s_c	r_∞
Transverse	MSD	1.06	1.96	1.31
	COMAC	0.44	3.99	1.77
Longitudinal	MSD	2.05	6.91	0.67
	COMAC	3.31	4.11	0.92
Diagonal 1	MSD	3.95	6.85	0.84
	COMAC	3.62	10.20	0.61
Diagonal 2	MSD	3.54	5.07	1.50
	COMAC	5.71	3.35	1.83

6. Discussion

From the results presented in section 5 it can be concluded so far that (1) the processing approach, based on a combination of wavelet de-noising and a two-dimensional Continuous Wavelet Transform, is capable of detecting damage and assessing geometric parameters down to signal-to-noise levels of 15 dB, (2) crack angles can be determined with high accuracy (to a fraction of a degree for transverse and longitudinal cracks, and with a bias of 1.5 – 2 degrees for diagonal cracks), (3) one characteristic fit parameter (the inverse of the square-root of the smaller of the eigenvalues of a quadratic form derived from the fit, see eq. (16)) can be reliably related to the crack length.

Referring to the last point, the measurement of the crack, we observe that crack length can be inferred from the analytical expression for the length ratio r, as given in eq. (13). The results for all fits have been summarized in Table 11, showing (a) the asymptotic length ratio r_∞, (b) the characteristic decay length s_c, and (c) the amplitude Δr.

It can be seen that the asymptotic length ratio r_∞ is similar for MSD and COMAC, though different results were obtained for cracks with different orientations. r_∞ is of the order of the unity, but variations by a factor of two between different orientations can be seen to occur. This angular dependence of may be attributed to the fact that the 2D-CW transform privileges one specific Cartesian coordinate system, which possibly translates into asymmetries between different orientations. In either case, it is clear that an order-of magnitude estimate of the crack length can be obtained from fitting $1/l_{crack}(s)$ to an exponentially expression, where $l_{crack}(s)$ is the characteristic length obtained at scale factor s, and extrapolating to $s\to\infty$. Then, the estimated value of the crack length is $\Delta l_{est} = r_\infty\, l_{crack,\infty} \sim l_{crack,\infty}$, since $r_\infty \sim 1$. A more systematic study will be presented in follow-up work.

Regarding the determination of the crack angle, an illustration of the key results have been plotted in Fig. 14. It can be seen that the overall prediction of the crack angle is fair, with the MSD method providing somewhat more accurate results. As illustrated by the comparison between the low-noise case on the left (SNR = 40dB) and the high-noise case on the right (SNR = 20dB), the method is quite insensitive to the noise level, making it potentially suitable for field applications.

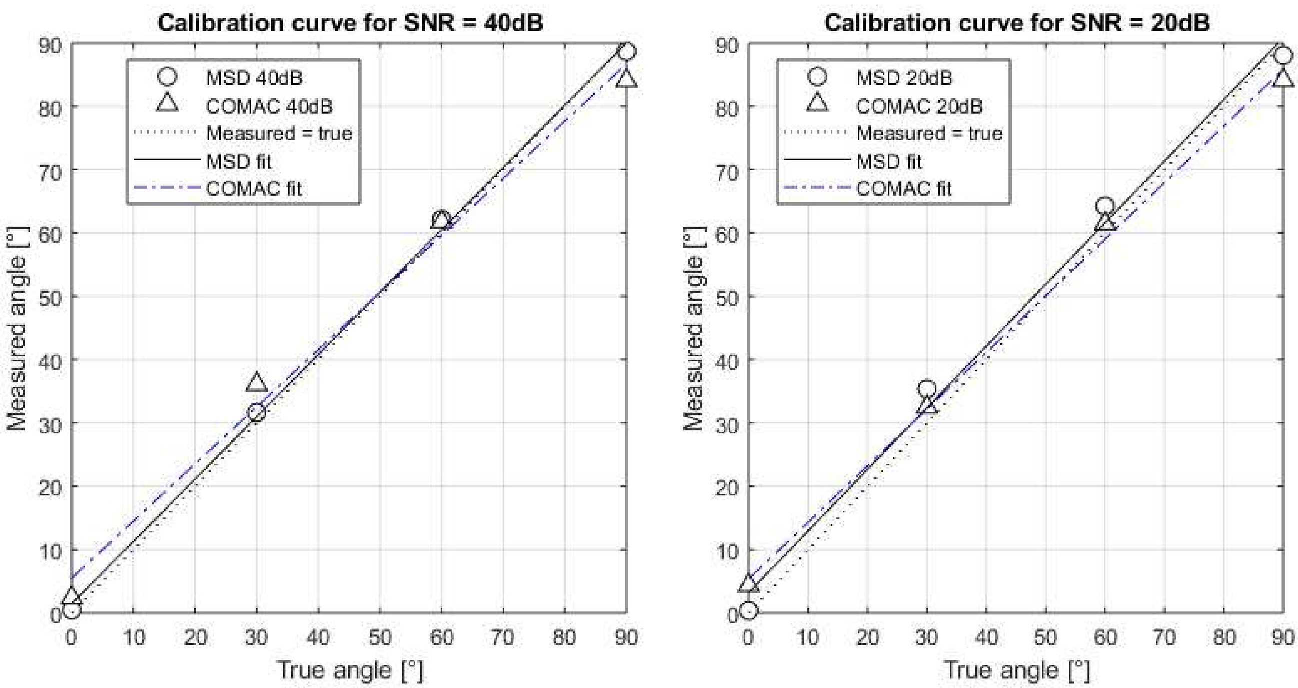

Fig. 14. Calibration curve for angle measurement with the MSD and the COMAC. The results on the left are for SNR=40dB, the ones on the right for SNR=20dB. As before, all results have been obtained with the combined de-noising / 2D-CWT method.

7. Summary and Conclusions

A new method has been proposed for the detection and geometrical characterization of crack-type faults in thin-walled beams made from composite material. The method is based on the analysis of the shapes of the normal modes of vibration of the beam as determined from modal analysis. Two metrics (Mode Shape Differences, MSD, and COMAC, Coordinate Modal Assurance Criterion) previously introduced in literature have been used to create spatial maps of damage. MSD and COMAC are able to detect crack-type faults under ideal conditions, but lose this ability at very low noise levels. In this work, a combined method has been proposed, which dramatically boots the capability of detecting and assessing damage, by combining a wavelet-based de-noising process with a two-dimensional Continuous Wavelet Transform (CWT) stage. Not only does this new approach allow faults to be detected down to signal-to-noise ratios of 15 dB, significantly lower than in most of the related work previously reported, but also can the geometry of the faults be assessed reliably. This assessment is based on a two-dimensional surface fitting approach, by which the damage signal is fitted to a bi-normal surface. This fitted surface can be used to assess both the length and the orientation of the crack; the crack width cannot be resolved. It was shown that an estimate of the crack length can be obtained by extracting a characteristic length of the larger dimension of the damage signal from the fit, conducting the fit for different scale factors of the CWT process, and extrapolating the results to infinite scale factors. In addition to the length of the crack, the angle can also be determined, by calculating the principal axes of the bi-normal fit surface. Both the length and the orientation are roughly independent of the noise level, as long as the damage signal can still be detected, i.e. down to SNR values of about 15 dB. Follow-up work will explore the parametric space of the problem more deeply, e.g. by assessing faults at a variety of locations, creating larger statistical ensembles for more consolidated results, and assessing the effect of using arbitrarily oriented coordinate systems for the 2D-CWT process used in this work.

Author Contributions

J. Pacheco-Chérrez conducted the finite-element simulations, implemented the different signal processing activities and generated all original data shown in this work. D. Cárdenas jointly designed the work plan with O. Probst, helped set up the finite-element simulations, and reviewed the results. O. Probst designed the project, together with D. Cárdenas, proposed the different processing steps, reviewed and analyzed the results, prepared the final figures, and wrote most of the manuscript.

Acknowledgments

JP is grateful for a PhD tuition scholarship from Tecnológico de Monterrey and a stipend for living expenses from CONACYT (Mexico). DC and OP acknowledge support from the Energy and Climate Change group at the School of Engineering and Sciences at Tecnológico de Monterrey.

Conflict of Interest

The authors declared no potential conflicts of interest with respect to the research, authorship, and publication of this article.

Funding

The authors received no financial support for the research, authorship, and publication of this article.

Nomenclature

a_{maj}	Major semi-axis of the elliptical cylinder [m]	(r, θ, z)	Cylindrical coordinates used with the sample surface
a_{min}	Minor semi-axis of the elliptical cylinder [m]	p	Circumferential coordinate at fixed z [m]
$\mathbf{A}$	Matrix representing the quadratic form (surface fit)	ψ	A mother wavelet
(b, e)	Center position of the crack (surface fit)	r_t	The length ratio $\Delta l/f$
COMAC	Coordinate Modal Assurance Criterion	r_l	The length ratio $\Delta l/c$
φ	A mode shape function	r_{diag}	The length ratio $\Delta l/l_{crack}$
Δl	Length of any of the cracks studied [m]	r_∞	The asymptotic value of a length ratio
λ_{12}	Eigenvalues of the argument of the surface fit [1/m]	s	The scale factor of the 2D CWT
l_{crack}	$1/\sqrt{\min(\lambda_2,\lambda_2)}$	s_c	A characteristic scale specifyin the decay of $r_{t,l,diag}$
MSD	Mode Shape Differences	SNR	Signal-to-noise ratio
		θ_{crack}	Measured crack orientation

References

[1] He, M., Yang, T., Du, Y., Nondestructive Identification of Composite Beams Damage Based on the Curvature Mode Difference, *Composite Structures*, 176, 2017, 178–86.

[2] Wang, K., Young, B., Smith, S. T., Mechanical Properties of Pultruded Carbon Fibre-Reinforced Polymer (CFRP) Plates at Elevated Temperatures, *Engineering Structures*, 33, (7), Elsevier Ltd, 2011, 2154–61.

[3] Thresher, R., Taking Advantage of Modern Turbines, *Nature Energy*, 3(6), 2018, 453–54.

[4] Abdulkareem, M., Bakhary, N., Vafaei, M., Noor, N. M., Mohamed, R. N., Application of Two-Dimensional Wavelet Transform to Detect Damage in Steel Plate Structures, *Measurement: Journal of the International Measurement Confederation*, 146, Elsevier Ltd, 2019, 912–23.

[5] Manoach, E., Warminski, J., Kloda, L., Teter, A., Numerical and Experimental Studies on Vibration Based Methods for Detection of Damage in Composite Beams, *Composite Structures*, 170, 2017, 26–39.

[6] Ganeriwala, S. N., Richardson, M., Using Modal Analysis for Detecting Cracks in Wind, *Technical Program for MFPT: The Applied Systems Health Management Conference 2011: Enabling Sustainable Systems*, (May), 2011, 10–13.

[7] Pastor, M., Binda, M., Harčarik, T., Modal Assurance Criterion, *Procedia Engineering*, 48, 2012, 543–48.

[8] Zhang, Y., Guo, J., Hao, N., Yang, J., Li, S., Damage Detection on Hull Girder of Ship Subjected to Explosion Loading, *Ocean Engineering*, 198, 2020, 107006.

[9] Altunışık, A. C., Okur, F. Y., Kahya, V., Modal Parameter Identification and Vibration Based Damage Detection of a Multiple Cracked Cantilever Beam, *Engineering Failure Analysis*, 79, 2017, 154–70.

[10] Hu, H., Wang, B. T., Lee, C. H., Su, J. S., Damage Detection of Surface Cracks in Composite Laminates Using Modal Analysis and Strain Energy Method, *Composite Structures*, 74(4), 2006, 399–405.

[11] Shahsavari, V., Chouinard, L., Bastien, J., Wavelet-Based Analysis of Mode Shapes for Statistical Detection and Localization of Damage in Beams Using Likelihood Ratio Test, *Engineering Structures*, 132, 2017, 494–507.

[12] Swamy, S., Reddy, D. M., Prakash G, J., Damage Detection and Identification in Beam Structure Using Modal Data and Wavelets, *World Journal of*

Modelling and Simulation, 13(1), 2017, 52–65.
[13] Janeliukstis, R., Rucevskis, S., Wesolowski, M., Chate, A., Multiple Damage Identification in Beam Structure Based on Wavelet Transform, *Procedia Engineering*, 172, 2017, 426–32.
[14] Serra, R., Lopez, L., Damage Detection Methodology on Beam-like Structures Based on Combined Modal Wavelet Transform Strategy, *Mechanics and Industry*, 18(8), 2017, 807.
[15] Zhu, L. F., Ke, L. L., Zhu, X. Q., Xiang, Y., Wang, Y. S., Crack Identification of Functionally Graded Beams Using Continuous Wavelet Transform, *Composite Structures*, 210, 2019, 473–85.
[16] Sha, G., Radzienski, M., Soman, R., Cao, M., Ostachowicz, W., Xu, W., Multiple Damage Detection in Laminated Composite Beams by Data Fusion of Teager Energy Operator-Wavelet Transform Mode Shapes, *Composite Structures*, 235, 2020, 111798.
[17] Makki Alamdari, M., Li, J., Samali, B., Damage Identification Using 2-D Discrete Wavelet Transform on Extended Operational Mode Shapes, *Archives of Civil and Mechanical Engineering*, 15(3), 2015, 698–710.
[18] Yang, C., Oyadiji, S. O., Delamination Detection in Composite Laminate Plates Using 2D Wavelet Analysis of Modal Frequency Surface, *Computers and Structures*, 179, 2017, 109–26.
[19] Skov, J. F., Ulriksen, M. D., Dickow, K. A., Kirkegaard, P. H., Damkilde, L., On Structural Health Monitoring of Wind Turbine Blades, *Key Engineering Materials*, 569–570, 2013, 628–35.
[20] Gökdağ, Y. E., Şansal, F., Gökdel, Y. D., Image Denoising Using 2-D Wavelet Algorithm for Gaussian-Corrupted Confocal Microscopy Images, *Biomedical Signal Processing and Control*, 54, 2019, 101594.
[21] Cho, D., Bui, T. D., Multivariate Statistical Modeling for Image Denoising Using Wavelet Transforms, *Signal Processing: Image Communication*, 20(1), 2005, 77–89.
[22] Huimin, C., Ruimei, Z., Yanli, H., Improved Threshold Denoising Method Based on Wavelet Transform, *Physics Procedia*, 33, 2012, 1354–59.
[23] Rucka, M., Wilde, K., Application of Continuous Wavelet Transform in Vibration Based Damage Detection Method for Beams and Plates, *Journal of Sound and Vibration*, 297(3–5), 2006, 536–50.
[24] Li, F., Meng, G., Kageyama, K., Su, Z., Ye, L., Optimal Mother Wavelet Selection for Lamb Wave Analyses, *Journal of Intelligent Material Systems and Structures*, 20(10), 2009, 1147–61.
[25] Reda Taha, M. M., Noureldin, A., Lucero, J. L., Baca, T. J., Wavelet Transform for Structural Health Monitoring: A Compendium of Uses and Features, *Structural Health Monitoring*, 5(3), 2006, 267–95.
[26] Yang, C., Oyadiji, S. O., Delamination Detection in Composite Laminate Plates Using 2D Wavelet Analysis of Modal Frequency Surface, *Computers and Structures*, 179, 2017, 109–26.

ORCID iD

Josué Pacheco-Chérrez https://orcid.org/0000-0003-0678-5091
Diego Cárdenas https://orcid.org/0000-0002-0512-6839
Oliver Probst https://orcid.org/0000-0003-0075-8295

How to cite this article: Pacheco-Chérrez J., Cárdenas D., Probst O. Measuring Crack-type Damage Features in Thin-walled Composite Beams using De-noising and a 2D Continuous Wavelet Transform of Mode Shapes, *J. Appl. Comput. Mech.*, 7(1), 2021, 355–371. https://doi.org/10.22055/JACM.2020.35156.2580